Cureus Journal of Engineering

Open Access Original Article

Agile Charging Methodology for Autonomous Underwater Vehicles Utilizing Inductor-Capacitor-Capacitor/Series-Series Compensation Topologies

Bassel ElFramawy [1] , Mariam Hossam [1] , Mariam Adel [1] , Peter Makeen [1]

1. Electrical Engineering, The British University in Egypt (BUE), Cairo, EGY

Corresponding authors: Mariam Hossam, mariam.hossam@bue.edu.eg, Mariam Adel, mariam.adel@bue.edu.eg, Peter Makeen, peter.makeen@bue.edu.eg

Received 03/27/2025
Review began 03/30/2025
Review ended 04/14/2025
Published 04/23/2025

© Copyright 2025
ElFramawy et al. This is an open access article distributed under the terms of the Creative Commons Attribution License CC-BY 4.0., which permits unrestricted use, distribution, and reproduction in any medium, provided the original author and source are credited.

DOI:
https://doi.org/10.7759/s44388-025-04043-8

Abstract

Wireless power transfer technology offers a flexible and efficient solution for recharging autonomous underwater vehicles (AUVs). However, rotational misalignments between the transmitter and receiver can significantly impact output power, charging current, and overall efficiency. This paper introduces a circular-arc-type magnetic coupler designed with a high tolerance for misalignment. Utilizing ANSYS Maxwell, a theoretical analysis of the magnetic field distribution, coupling coefficient, and mutual inductance between the transmitter and receiver for this innovative design is conducted. Additionally, an Inductor-Capacitor-Capacitor/Series-Series resonant compensation topologies are presented to facilitate rapid charging of the AUV's battery, maintaining optimal current and efficiency across a range of rotational misalignments [−10° to 10°] and axial misalignments [−30 mm to 30 mm]. An increase in the charging current of 7.01% concerning the rotational misalignment is achieved by implementing the proposed manipulated switching compensation topologies. The proposed approach demonstrates exceptional adaptability, achieving an output power of 4.185 kW with an efficiency of 95.05%. The theoretical results align closely with existing literature, underscoring the effectiveness of the proposed methodology.

Categories: Energy Efficiency and Conservation, Vehicle Dynamics and Control, Power Electronics and Renewable Energy
Keywords: wireless power transfer, annular coil, autonomous underwater vehicle, compensation topology, circular-arc-type

Introduction

Recent advances in marine exploration have centered on autonomous underwater vehicles (AUVs). Advances in battery capacity and hydrogen fuel cells enable AUVs to complete lengthier missions than remotely operated vehicles. AUVs are becoming increasingly important in scientific, commercial, and military applications. Due to the absence of physical attachment, AUVs may carry out missions throughout a greater territory, necessitating the employment of more current navigation systems to get precise location estimations during deployment, operation, charging, and retrieval [1-3]. AUVs may be charged in two ways: through battery swapping and wireless charging. Battery switching involves replacing a depleted battery with a fully charged one. However, it is difficult to implement and requires retrieval methods [4]. Furthermore, frequent swapping may jeopardize the airtightness of AUVs.

To overcome the energy issue and enable AUVs to operate long-term, magnetically linked resonant wireless power transfer (WPT) technology has been proposed. However, the natural topology of ocean currents considerably effects the misalignment between the transmitter and receiver, thereby directly influencing the stability and efficiency of power transfer. To tackle this issue, researchers are directed to improve the WPT network, as has been addressed and investigated in the literature review articles [5]. The core components of the WPT systems are the magnetic coupler (MC) and compensation topology network. The MC is directly determining the magnetic field patterns and link's performance. There are different structures that have been utilized in the inductive WPT system concerning the AUV, such as circular-ring, coaxial-coil, semi-closed magnetic core, spiral structure, curly-coil structure, fit-to-surface, H-type, dipole-arc-type, cone-type, R-type, and three-phase-R-type, and circular-arc-type (CA-type) [5]. However, the CA-type structure ensured perfect dynamic behavior, easy to forge and install, lightweight receiver, and anti-misalignment tolerance concerning the mentioned types in [6]. The second component, which is considered the complementary of the MC, is the compensation topology network that reduces the transmission system loss and increases the system transmission power, such as Series-Series (S-S), Series-Parallel (S-P), Parallel-Series (P-S), Parallel-Parallel (P-P), Inductor-Capacitor-Capacitor Series (LCC-S), Inductor-Capacitor-Capacitor Inductor-Capacitor-Capacitor (LCC-LCC), and Inductor-Capacitor-Capacitor Series-Parallel (LCC-SP), as stated in detail in [7-11]. Therefore, every research article suggested a combined system incorporating both the MC and compensation topology networks.

How to cite this article
ElFramawy B, Hossam M, Adel M, et al. (April 23, 2025) Agile Charging Methodology for Autonomous Underwater Vehicles Utilizing Inductor-Capacitor-Capacitor/Series-Series Compensation Topologies. Cureus J Eng 2 : es44388-025-04043-8. DOI https://doi.org/10.7759/s44388-025-04043-8

In [12], a new coil design featuring two decoupled receivers made up of two oppositely wound receiver coils with their magnetic flux directions-oriented perpendicular has been proposed. The LCC-LCC compensated topology was utilized, where the system ensured 485 W with 92.26% DC-DC efficiency. However, the natural topology of ocean currents considerably affects the misalignment between the transmitter and receiver, thereby directly influencing the stability and efficiency of power transfer. In [13], a coil formed out of three identical transmitters and one receiver-two components connected in series-provided 745 W with an LCC-LCC compensation topology, guaranteeing an 86.19% DC-DC efficiency. In [14], using two transmitters and one receiver supported by cubic ferrite, a free-rotation WPT magnetic coupler was suggested. For a 700 W output power system, this design improved the axial and rotational misalignments with a fluctuation of less than 5%. However, the transmitter and receiver must both contain ferrite for this method to work. A coreless, annular-coupled WPT system with an S-P compensation topology was created that transferred 300 W in [15] and ensured 77% efficiency. By using a compensation topology that is LCC-S, the authors in [16] demonstrated an inductive power transfer system compatible with AUV hulls can achieve a power transfer of 5.180 kW in a downscaled prototype with an 80-kW power rating and 93.9% efficiency. In [4], the magnetic field distribution of a three-phase wireless charging system based on an annular magnetic coupler can transmit 1 kW of electricity at 465 kHz with 92.41% efficiency. In [17], studies demonstrated that in saltwater, annular coil-based wireless charging devices can achieve up to 90% efficiency at 680 W. To highlight the originality of this paper, and based on an ongoing literature assessment, Table *1* compares the several WPT systems used in AUVs to demonstrate the novelty of this work. Coil design, operating frequency, output power, system efficiency, compensatory topologies, axial and rotational misalignments, and load characteristics are all included in this analysis.

Ref	Coil Design Structures	Freq. (kHz)	Output Power (W)	System Efficiency (%)	Compensation Topology	Axial Misalignment (mm)	Rotational Misalignment (°)	Load
[18]	Arc-shaped	85	3,000	91.9%	LCC-LCC	[0 mm, 20 mm]	[0°, 10°]	Resistive (14.4 Ω)
[19]	Variable ring-shaped	100	300	86% (air) 85.72 % (water)	LCC-S	—	—	Resistive (6 Ω)
[20]	“Overlapped direct-quadrature transmitter and a dipole receiver”	85	1,200	90%	LCC-P	[−30 mm, 30 mm]	[−30°, 30°]	Resistive
[21]	“Arc bipolar transmitter and a compact dipole-coil-based receiver”	50	1,000	95.1%	LCC-S	[−30 mm, 30 mm]	[−10°, 10°]	Lithium-ion battery (11A, 54 V)
[22]	Variable ring-shaped	100	800	86.4%	LCC-S	20 mm	10°	Resistive (15 Ω)
[23]	H-shaped	85	735.6	90.87%	LCC-P	[−25 mm, 25 mm]	[−10°, 10°]	Resistive (16 Ω)
[6]	Circular-arc	50	575	92.51%	S-P	[−30 mm, 30 mm]	[−10°, 10°]	Resistive (20 Ω)
[24]	E-type	76	120	96%	LCC-S	[−30 mm, 30 mm]	[−10°, 10°]	Resistive (50 Ω)
[25]	U-shaped bipolar coil transmitter and an arc-shaped unipolar receiver	85	500	88%	LCC-S	[0 mm, 60 mm]	[−45°, 45°]	Resistive (10 Ω to 50 Ω)
This Work	Circular arc (CA)	50	4185	95.05%	LCC/S-S	[−30 mm, 30 mm]	[−10°, 10°]	Battery (300 V, 10 Ah)

TABLE 1: Comparison between various WPT systems implemented in the AUVs’ applications

WPT, Wireless power transfer; AUV, autonomous underwater vehicle; LCC-LCC, Inductor-Capacitor-Capacitor Inductor-Capacitor-Capacitor; LCC-S, Inductor-Capacitor-Capacitor/Series; LCC-P, Inductor-Capacitor-Capacitor-Parallel; S-P, Series-Parallel; LCC/S-S, Inductor-Capacitor-Capacitor/Series-Series

In order to greatly increase misalignment tolerance for wireless AUV charging this research presents a novel WPT system composed of a magnetic coupler. The performance of a CA-type magnetic coupler under varied misalignment settings is the main topic of the study. The main contribution of this study is

the suggestion of a novel compensation topology that combines the S-S and LCC-S topologies while adjusting the switch state, providing an entirely novel perspective on power transmission and efficiency optimization.

Materials And Methods

WPT system principle analysis

The mutual inductance (M) and coupling coefficient (K) parameters are crucial for evaluating the magnetic coupler in a WPT system since they have an impact on power transmission and coupling efficiency. The total WPT system with LCC/S-S compensation is shown in Figure *1* to investigate the relationship between output power and M.

This system uses an AC input power supply of 325 V and 50 Hz followed by a rectifier and H-bridge inverter with 4 controlled Mosfets and antiparallel diodes to generate high-frequency AC power. A compensation capacitor CP, CLLC-1, and CLLC-2 are chosen to match its impedance with the primary side inductance Lp and parasitic internal resistance Rp at the operating frequency that is set to 50 kHz. This configuration allows the current to resonate and generate a high magnetic flux density, with the majority of the flux going through the receiver coil. The compensation network helps to lower the VA rating of the power supply for the given battery load by ensuring that the switches handle only real power. Additionally, a series compensation capacitor CS is selected to match the secondary side inductance LS and parasitic internal resistance RS at the operating frequency. The vehicle rectifier in the secondary circuit, composed of 4 diodes, provides the output voltage and current to the battery. The WPT system is simulated using MATLAB-Simulink, and the magnetic coupler is simulated with ANSYS Maxwell. A clear investigation of the compensation circuit zone, including a scrutinizing analysis of the compensation topology and magnetic coupler, will be discussed in the following subsections.

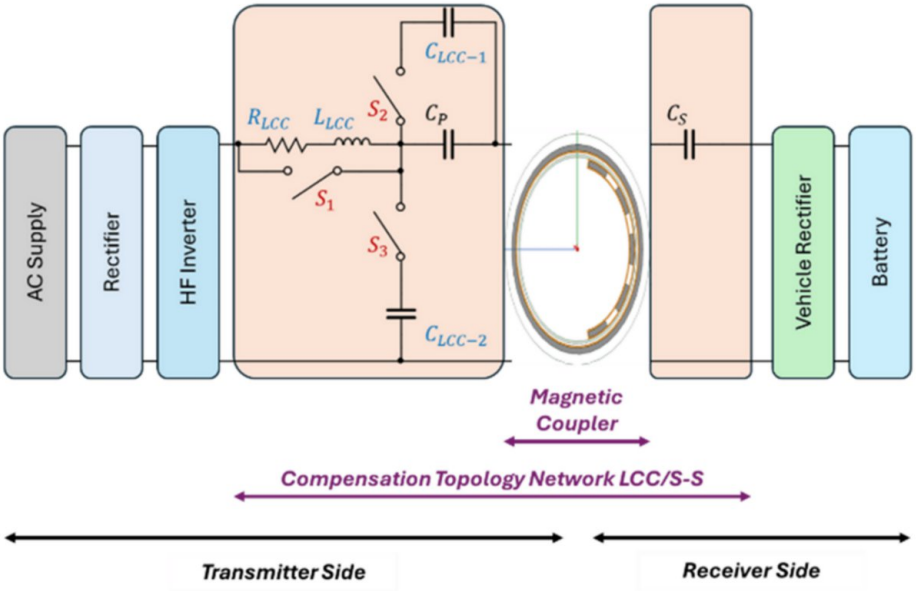

FIGURE 1: WPT system with LCC/S-S compensation topology for charging AUV batteries

WPT, wireless power transfer; LCC/S-S, Inductor-Capacitor-Capacitor/Series-Series; AUV, autonomous underwater vehicle

Magnetic coupler design

The AUV in this study is considered to have an outer diameter of 300 mm; hence, the internal diameter of the docking station should be greater than or equal to 330 mm. The transmitter was fixed to the docking station and considered to be 330 mm, as stated in [6]. The dimensions and parameters of the CA-type are listed in Table *2*. Because of the difficult forging of the annular ferrite material of the transmitter, the primary core was set as 6 circular-arc cores with a central angle of 60 as mentioned in [6]. The magnetic coupler of WPT systems depends on the coupling state and power transmission capability, which are influenced by K and M parameters. The overall structure of the magnetic coupler was established using ANSYS Maxwell, as shown in Figure *2*.

Parameters	Value
L = length of the magnetic core (mm)	50
W = width of the magnetic coupler for both the transmitter and receiver inside the paper (mm)	100
H = thickness of the magnetic core (mm)	10
θ_1 = central angle of a single receiver core (°)	20
θ_2 = The angle between the receiver cores (°)	14
N_r = Number of turns of the receiver cores (turn)	5
R_{T1} = outer radius of transmitter (mm)	170.8
R_{T2} = inner radius of the transmitter (mm)	160.8
R_{R1} = outer radius of receiver (mm)	147.2
R_{R2} = inner radius of the receiver (mm)	137.2
NP = number of turns of the transmitter (turn)	9
NS = number of turns of the receiver (turn)	13
D = wire diameter (mm)	2.8

TABLE 2: Parameters of the circular-arc-type

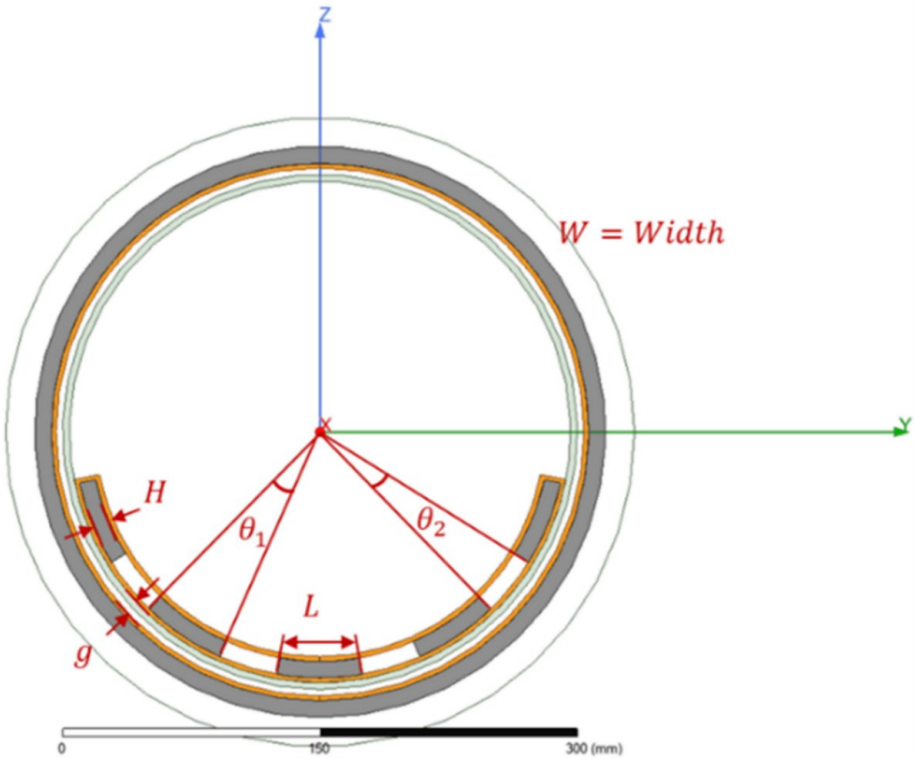

FIGURE 2: Schematic diagram of the circular-arc-type structural design

Proposed compensation topology network design

In this study, the LCC-S and S-S compensation topologies were utilized to ensure maximum efficiency between the transmitter and receiver, while the working principle analysis is discussed [26] and will be

summarized in the following subsections. The S-S and LCC-S topologies have been widely used because of their simple structure, robustness, and insensitivity to the coupling coefficient with the intrinsic short-circuit protection [27]. Self-switching between the mentioned compensation topologies has been designed to improve the transmission performance and various conditions. The schematic topology network of the self-switching system is illustrated in Figure 3, which depends on the controlled switches, S_1, S_2, and S_3. The parameters of each topology such as the capacitors, inductors, their parasitic resistances, and the arrangement of switches are investigated in the following subsections.

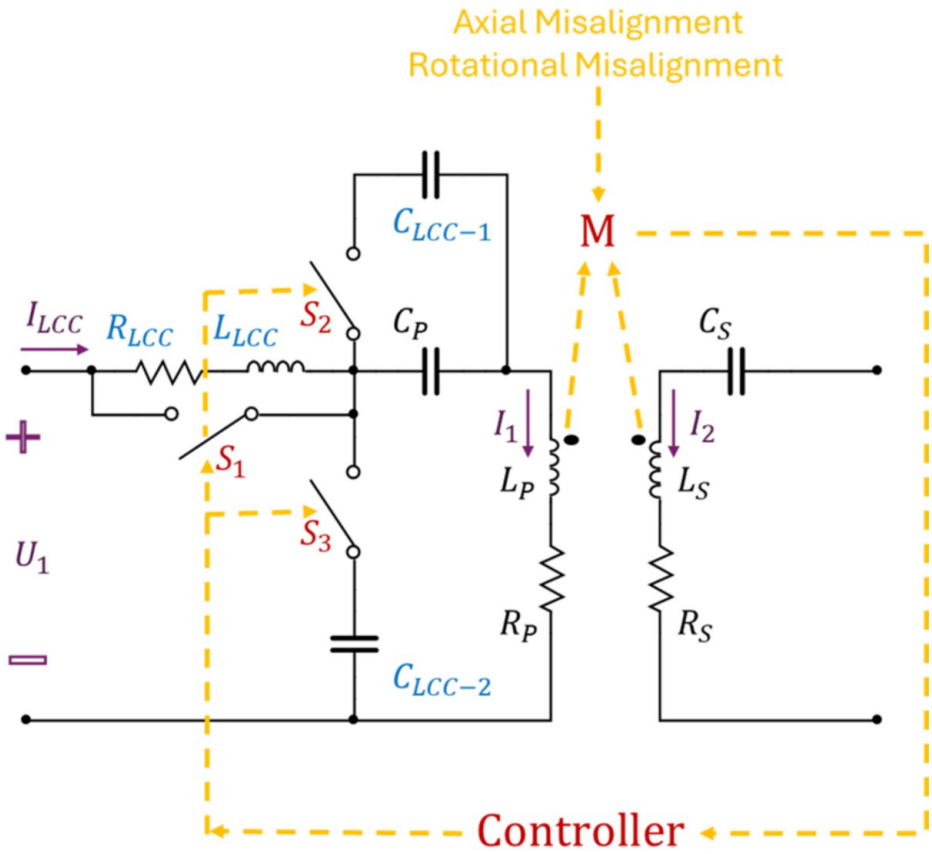

FIGURE 3: The proposed self-switching WPT compensation topology network

WPT, wireless power transfer

S-S compensation topology

The S-S topology is implemented when S_1 is closed and S_2 and S_3 are disconnected. In resonance, the supply angular frequency should be equal to the angular frequencies of the transceiver, as represented in equation (1). The equivalent resistance of the vehicle rectifier could be represented as in equation (2), which depends on the load resistance.

$$\omega = \frac{1}{\sqrt{C_P L_P}} = \frac{1}{\sqrt{C_S L_S}} \quad (1)$$

$$R = \frac{8R_L}{\pi^2} \quad (2)$$

Where, C_P and C_S are the capacitors in the primary and secondary coils, respectively, L_P and L_S represent the inductance of the transmitter and receiver coils, respectively. R_L is the load resistance, and R is the equivalent resistance of the rectifier bridge.

Based on Kirchhoff's Voltage law, the loop equation of the input voltage of the compensation topology

circuit is represented by equation (3), and the loop equation of the secondary circuit is represented by equation (4). While the currents passing through the coupler could be represented by equations (5) and (6), respectively.

$$U_1 = \left(R_P + j\omega L_P + \frac{1}{j\omega C_P}\right) I_1 - j\omega M I_2 \quad (3)$$

$$-RI_2 = j\omega M I_1 + \left(R_S + j\omega L_S + \frac{1}{j\omega C_S}\right) I_2 \quad (4)$$

$$I_1 = \frac{(R_S + R)U_1}{(\omega M)^2 + R_P(R_S + R)} \quad (5)$$

$$I_2 = \frac{j\omega M U_1}{(\omega M)^2 + R_P(R_S + R)} \quad (6)$$

Where, U_1 is the input voltage and M is the mutual inductance between the transmitter and receiver.

Consequently, the input and output powers and efficiency are represented as follows:

$$P_{in} = \frac{(R_S + R)U_1^2}{R_P(R_S + R) + (\omega M)^2} \quad (7)$$

$$P_{out} = \frac{R(\omega M)^2 U_1^2}{[R_P(R_S + R) + (\omega M)^2]^2} \quad (8)$$

$$\eta = \frac{R(\omega M)^2}{[R_P(R_S + R) + (\omega M)^2](R_S + R)} \quad (9)$$

LCC-S compensation topology

The LCC-S topology was implemented when S_2 and S_3 were closed and S_1 is opened. In resonance, the transmitter and receiver angular frequencies should be equal as represented in equations (10) and (11).

$$\omega L_P - \frac{1}{\omega(C_P + C_{LCC-1})} = \frac{1}{\omega C_1} = \omega L_{LCC} \quad (10)$$

$$\omega L_S = \frac{1}{\omega C_S} \quad (11)$$

The voltage, current equations for both the primary and secondary loop circuits are expressed in equations (12) to (17).

$$U_1 = (R_{LCC} + j\omega L_{LCC}) I_{LCC} + \left(R_P + j\omega L_P + \frac{1}{j\omega C_P}\right) I_1 + j\omega M I_2 \quad (12)$$

$$\left(R_P + j\omega L_P + \frac{1}{j\omega C_P}\right) I_1 + j\omega M I_2 = \frac{1}{j\omega C_{LCC-2}}(I_{LCC-2} - I_1) \quad (13)$$

$$-RI_2 = \left(R_S + j\omega L_S + \frac{1}{j\omega C_S}\right) I_2 + j\omega M I_1 \quad (14)$$

$$I_1 = \frac{U_1}{j\omega C_{LCC-2} R_{LCC} A} \quad (15)$$

$$I_2 = \frac{-MU_1}{C_{LCC-2} R_{LCC}(R + R_S)A} \quad (16)$$

$$I_{LCC} = \frac{U_1}{R_{LCC}} - \frac{U_1}{(\omega C_{LCC-2} X R_{LCC}) A^2} \quad (17)$$

Where,

$$A = R_P + \frac{(\omega M)^2}{R + R_S}$$

At this point, the input and output powers and the efficiency are concluded in equations (18), (19), and (20).

$$P_{in} = \frac{U_1^2}{R_{LCC}} = \frac{U_1^2}{(\omega C_{LCC-2} R_{LCC}) A^2} \quad (18)$$

$$P_{out} = \frac{(MU_1)^2 R}{C_{LCC-2} R_{LCC}^2 (R + R_S)^2 A^2} \quad (19)$$

$$\eta = \frac{(MU_1)^2 R}{A(R + R_S)(\omega^2 C_{LCC-2} R_{LCC} (R + R_S)^2 A - 1)} \quad (20)$$

The internal resistance of the LCC is very small so it can be neglected as in [28]. In both topologies, the load is considered a lithium-ion battery with dynamic behavior, where such batteries have different internal resistances based on the corresponding state of charge (SOC), as stated in [29,30].

Results

When the AUV is docked and charged, some degree of misalignment of the magnetic coupler is unavoidable. This misalignment can be classified into three types: rotational, axial, and radial. Given that the AUV is secured by a clamping mechanism when it docks on the seabed, radial misalignment is less concerning. Therefore, this study focused on the effects of rotational and axial misalignments. Typically, recharging docks are situated in areas with relatively calm ocean currents, and AUVs are equipped with a self-stabilizing mechanism that minimizes significant rotational and axial misalignments. Consequently, finite element analysis was conducted on the CA-type coil using ANSYS Maxwell, considering rotational misalignment ranging from −10° to 10° and axial misalignment ranging from −30 mm to 30 mm, as outlined by the optimization parameters. In this section, all findings are investigated to reveal the novelty of the proposed controlled system started from the magnetic field distribution of the proposed magnetic coupler.

Magnetic field distribution

The magnetic field distribution of a CA coil is influenced by the geometry of the coil and the current flowing through it. For a CA-type, the field lines tend to be concentrated near the coil, creating a magnetic field that follows the curvature of the arc. The proposed design aimed to produce an efficient magnetic field distribution, as shown in Figure *4*, where the maximum magnetic field reached 45.27 mT. Besides, the simulation parameters of the circular-arc-type and LCC/S-S compensation topology network circuits are presented in Table *3*.

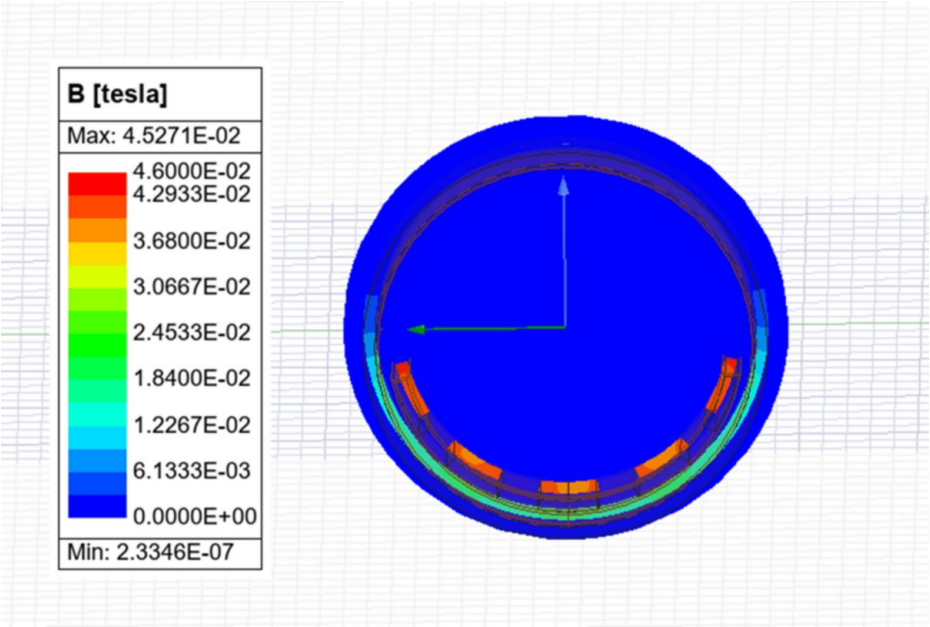

FIGURE 4: The magnetic field distribution of the circular-arc-type

Parameters	Value
C_P = capacitance of the S compensation topology in the primary circuit (μF)	0.16
C_{LCC-1} = capacitance of the LCC compensation topology (μF)	0.188
C_{LCC-2} = capacitance of the LCC compensation topology (μF)	0.296
L_{LCC} = inductance of the LCC compensation topology (μH)	34.3
C_S = capacitance of the S compensation topology in the secondary circuit (nF)	98.1
Li-ion battery voltage (V)	300
Li-ion battery rated capacity (Ah)	10
Li-ion battery initial SOC (%)	50
L_P = transmitter's self-inductance (μH)	63.50
R_P = resistance of the transmitter coil (Ω)	0.25
L_S = receiver's self-inductance (μH)	103.38
R_S = resistance of the receiver coil (Ω)	0.25
M = mutual inductance (μH)	52.99
k = coupling coefficient	0.66

TABLE 3: Simulation parameters of the CA-type and LCC/S-S compensation topology network circuit

Rotational and axial misalignments

The impact of rotational and axial misalignments on the coupling coefficient (K) and mutual inductance (M) is illustrated in Figure *5*. Figure *5a* and b show the effects of rotational misalignment, indicating that the proposed CA-type magnetic coupler maintains strong stability within a rotation angle range of [−10°, 10°]. The ripples in both K and M are minimal, measuring less than 0.0013 and 0.23 μH, respectively.

Conversely, Figure 5c and d depict the effects of axial misalignment. These figures reveal that an axial displacement within the range of [−30 mm, 30 mm] significantly impacts both K and M. Specifically, as the misalignment increases from 0 to 30 mm, K decreases from 0.658 to 0.52, while M decreases from 52.99 μH to 35.11 μH.

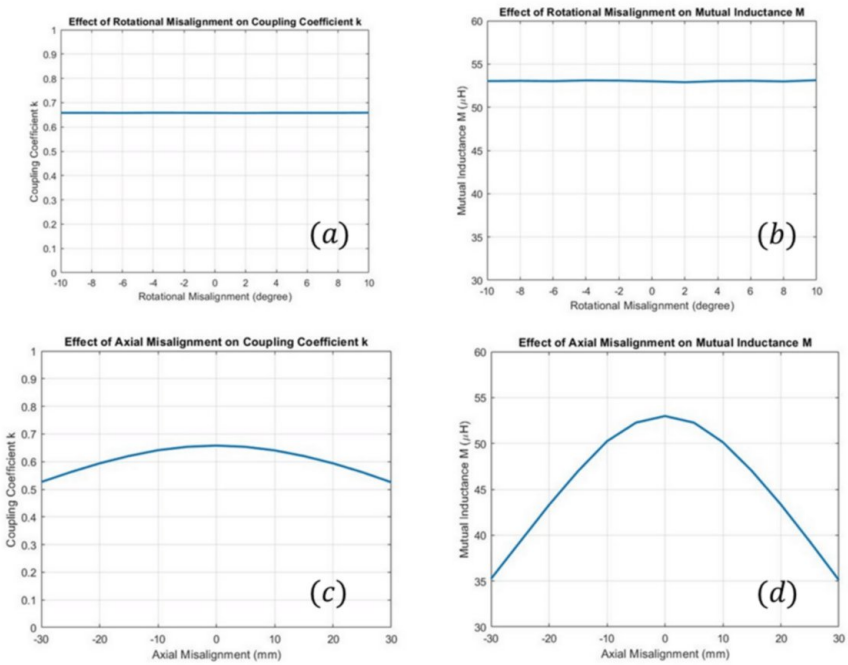

FIGURE 5: (a and b) Impact of the rotational misalignment on the coupling coefficient and mutual inductance, respectively; (c and d) impact of the axial misalignment on the coupling coefficient and mutual inductance, respectively

Discussion

The proposed LCC/S-S compensation topology

The proposed LCC/S-S compensation topology is designed to achieve maximum output power and efficiency for charging lithium-ion batteries. To optimize performance across the entire range of axial and rotational misalignments, a dynamic design approach is recommended. This approach utilizes a controller that can switch between the S and LCC topologies in the main circuit, dependent on the degree of detected axial and rotational misalignment. Using this adaptive switching mechanism, the system may capitalize on the better properties of each topology in their respective ideal zones, therefore maximizing total output current and efficiency under varied misalignment circumstances.

In the axial misalignment operation, the output current behavior of the S and LCC topologies revealed differential performance characteristics across different areas of misalignment. The S-S topology offers a larger output current of 12.4 A between −30 mm and −6.4 mm, as well as between 6.4 mm and 30 mm. In the intermediate zone of −6.4 mm to 6.4 mm, the LCC topology excels with a maximum output current of 13.21 A, as shown in Figure 6a.

Examining the output current in relation to the rotational misalignment reveals that the LCC topology outperforms the SS topology, as shown in Figure 6b. This had a maximum output current of 13.21 A. The LCC topology design efficiently adjusts for differences in alignment, resulting in a more stable output current despite rotational misalignment. This better stability can be due to its intrinsic capacity to compensate for misalignment, which results in lower losses and more efficiency. As a result, the LCC architecture performs more consistently and robustly in cases where rotational misalignment is a problem, making it a superior alternative for applications using circular arc coils in underwater vehicles.

When we investigated the efficiency of the various topologies in response to axial misalignment, we discovered differential performance profiles for the S and LCC compensation topologies. The SS topology has a greater efficiency of 88.5% for axial misalignment ranges of −25 mm to −30 mm and 25 mm to 30 mm. Figure 6c shows that the LCC topology performs best in the middle range of −25 mm to 25 mm, with a maximum efficiency of 95%.

In terms of rotational misalignment, the LCC topology clearly outperforms the SS topology, with a maximum efficiency of 95%, as indicated in Figure *6d*. The LCC's design successfully compensates for alignment variations, which improves total system efficiency. Thus, the LCC architecture provides more reliable and durable performance for applications with rotational misalignment difficulties, making it a superior alternative for systems like circular-arc coils in underwater vehicles.

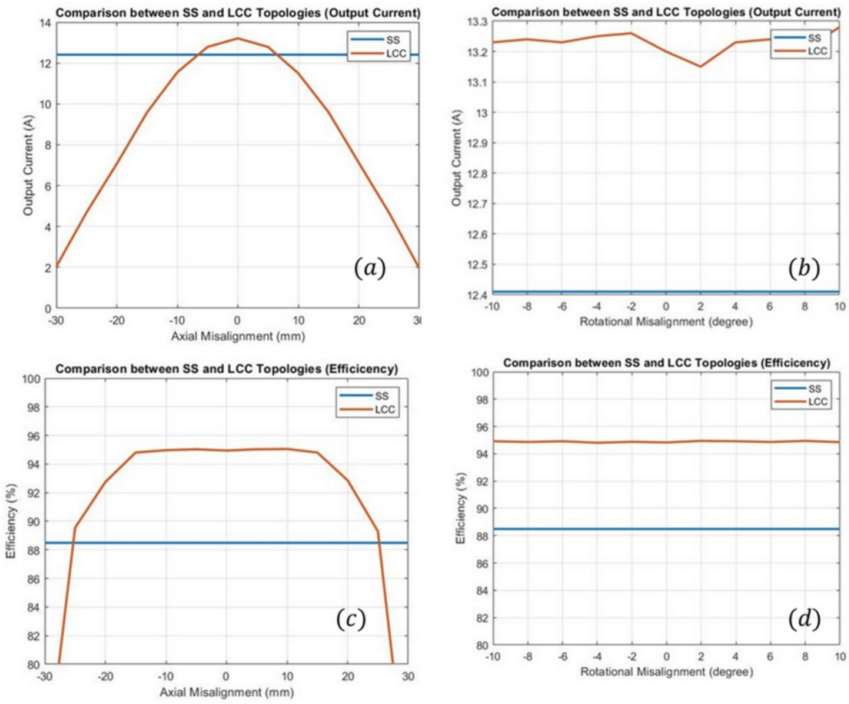

FIGURE 6: Comparison between the LCC-S and S-S compensation topologies: (a and b) output current regarding the axial and rotational misalignments, respectively; (c and d) efficiency regarding the axial and rotational misalignments, respectively

LCC-S, Inductor-Capacitor-Capacitor Series; S-S, Series-Series

Conclusions

This research presents a novel CA-type magnetic coupler that significantly enhances the WPT capabilities of AUVs. By addressing the challenges caused by rotational and axial misalignments, the proposed system has a high tolerance for misalignment, resulting in a constant power supply. The theoretical study done with ANSYS Maxwell shows that the CA-type coupler has a favorable magnetic field distribution, coupling coefficient, and mutual inductance. Furthermore, the implementation of an LCC/S-S resonant compensation architecture enables for quicker battery charging while maintaining optimal current and efficiency under diverse misalignment circumstances. The charging current reached 12.41 A with the S-S topology, compared to 2.035 A with the LCC-S in axial misalignment and 13.28 A instead of 12.41 A when using the LCC-S in rotational misalignment. With an astonishing output power of 4185 W and an impressive efficiency of 95.05%, the suggested technique not only satisfies the operational needs of AUVs but also fits well with previous research, as presented in the literature study. This study provides critical insights into the advancement of WPT technology for more efficient and adaptable AUV systems.

Future work is going to concentrate on experimental validation and the creation of an implementation strategy that includes hardware integration, control optimization, and thermal management. Key technical issues such as electromagnetic compatibility, parasitic losses, underwater insulation, and long-term operational stability under marine circumstances will be addressed in a systematic manner to provide dependable and efficient deployment in AUV environments.

Additional Information

Author Contributions

All authors have reviewed the final version to be published and agreed to be accountable for all aspects of the work.

Concept and design: Peter Makeen, Mariam Adel, Mariam Hossam, Bassel ElFramawy

Acquisition, analysis, or interpretation of data: Peter Makeen, Mariam Adel, Mariam Hossam, Bassel ElFramawy

Drafting of the manuscript: Peter Makeen, Mariam Adel, Mariam Hossam, Bassel ElFramawy

Critical review of the manuscript for important intellectual content: Peter Makeen, Mariam Adel, Mariam Hossam, Bassel ElFramawy

Supervision: Peter Makeen

Disclosures

Human subjects: All authors have confirmed that this study did not involve human participants or tissue. **Animal subjects:** All authors have confirmed that this study did not involve animal subjects or tissue. **Conflicts of interest:** In compliance with the ICMJE uniform disclosure form, all authors declare the following: **Payment/services info:** All authors have declared that no financial support was received from any organization for the submitted work. **Financial relationships:** All authors have declared that they have no financial relationships at present or within the previous three years with any organizations that might have an interest in the submitted work. **Other relationships:** All authors have declared that there are no other relationships or activities that could appear to have influenced the submitted work.

References

1. Zhang B, Ji D, Liu S, Zhu X, Xu W: Autonomous Underwater Vehicle navigation: a review. Ocean Engineering. 2023, 273:113861. 10.1016/j.oceaneng.2023.113861
2. Yang Y, Xiao Y, Li T: A survey of autonomous underwater vehicle formation: performance, formation control, and communication capability. IEEE Communications Surveys & Tutorials. 2021, 23:815-41. 10.1109/comst.2021.3059998
3. He Y, Wang DB, Ali ZA: A review of different designs and control models of remotely operated underwater vehicle. Measurement and Control. 2020, 53:1561-70. 10.1177/0020294020952483
4. Kan T, Mai R, Mercier PP, Mi CC: Design and analysis of a three-phase wireless charging system for lightweight autonomous underwater vehicles. IEEE Transactions on Power Electronics. 2018, 33:6622-32. 10.1109/tpel.2017.2757015
5. Yang L, Li X, Zhang Y, et al.: A review of underwater inductive wireless power transfer system. IET Power Electronics. 2023, 17:894-905. 10.1049/pel2.12456
6. Xia T, Li H, Yu H, Zhang Y, Hu P: A circular-arc-type magnetic coupler with strong misalignment tolerance for AUV wireless charging system. Journal of Marine Science and Engineering. 2023, 11:162. 10.3390/jmse11010162
7. Sagar A, Kashyap A, Nasab MA, Padmanaban S, Bertoluzzo M, Kumar A, Blaabjerg F: A comprehensive review of the recent development of wireless power transfer technologies for electric vehicle charging systems. IEEE Access. 2023, 11:83703-751. 10.1109/access.2023.3300475
8. Vu VB, Ramezani A, Triviño A, et al.: Operation of inductive charging systems under misalignment conditions: a review for electric vehicles. IEEE Transactions on Transportation Electrification. 2023, 9:1857-87. 10.1109/tte.2022.3165465
9. Shanmugam Y, Narayanamoorthi R, Vishnuram P, Bajaj M, AboRas KM, Thakur P, Kitmo: A systematic review of dynamic wireless charging system for electric transportation. IEEE Access. 2022, 10:133617-3642. 10.1109/access.2022.3227217
10. Venkatesan M, Rajamanickam N, Vishnuram P, Bajaj M, Blazek V, Prokop L, Misak S: A review of compensation topologies and control techniques of bidirectional wireless power transfer systems for electric vehicle applications. Energies. 2022, 15:7816. 10.3390/en15207816
11. Rayan BA, Subramaniam U, Balamurugan S: Wireless power transfer in electric vehicles: a review on compensation topologies, coil structures, and safety aspects. Energies. 2023, 16:3084. 10.3390/en16073084
12. Yan Z, Song B, Zhang Y, Zhang K, Mao Z, Hu Y: A rotation-free wireless power transfer system with stable output power and efficiency for autonomous underwater vehicles. IEEE Transactions on Power Electronics. 2019, 34:4005-8. 10.1109/tpel.2018.2871316
13. Kan T, Zhang Y, Yan Z, Mercier PP, Mi CC: A rotation-resilient wireless charging system for lightweight autonomous underwater vehicles. IEEE Transactions on Vehicular Technology. 2018, 67:6935-42. 10.1109/tvt.2018.2836988
14. Yan Z, Wu M, Zhao C, Hu Q, Zhu L, Qiao L, Wang L: Free-rotation wireless power transfer system based on composite anti-misalignment method for AUVs. IEEE Transactions on Power Electronics. 2023, 38:4262-66. 10.1109/tpel.2023.3238066
15. Lin M, Li D, Yang C: Design of an ICPT system for battery charging applied to underwater docking systems. Ocean Engineering. 2017, 145:373-81. 10.1016/j.oceaneng.2017.08.002
16. Mostafa A, Wang Y, Zhang H, Tangirala S, Lu F: An ultra-fast wireless charging system with a hull-compatible coil structure for autonomous underwater vehicles (AUVs). IEEE Transportation Electrification Conference & Expo (ITEC), Anaheim, CA, USA. 2022, 279-84. 10.1109/ITEC53557.2022.9813911
17. Yang C, Lin M, Li D: Improving steady and starting characteristics of wireless charging for an AUV docking system. IEEE Journal of Oceanic Engineering. 2020, 45:430-41. 10.1109/joe.2018.2872449
18. Wang DA, Cui S, Zhang J, Bie Z, Song K, Zhu C: A novel arc-shaped lightweight magnetic coupler for AUV wireless power transfer. IEEE Transactions on Industry Applications. 2022, 58:1315-29.

10.1109/tia.2021.3109839
19. Zhang B, Wang X, Lu C, Lu Y, Xu W: A wireless power transfer system for an autonomous underwater vehicle based on lightweight universal variable ring-shaped magnetic coupling. International Journal of Circuit Theory and Applications. 2023, 51:2654-73. 10.1002/cta.3568
20. Wu S, Cai C, Wang A, Qin Z, Yang S: Design and implementation of a uniform power and stable efficiency wireless charging system for autonomous underwater vehicles. IEEE Transactions on Industrial Electronics. 2023, 70:5674-84. 10.1109/TIE.2022.3198242
21. Cai C, Wu S, Zhang Z, Jiang L, Yang S: Development of a fit-to-surface and lightweight magnetic coupler for autonomous underwater vehicle wireless charging systems. IEEE Transactions on Power Electronics. 2021, 36:9927-40. 10.1109/tpel.2021.3064411
22. Zhang B, Chen J, Wang X, Xu W, Lu C, Lu Y: High-power-density wireless power transfer system for autonomous underwater vehicle based on a variable ring-shaped magnetic coupler. IEEE Transactions on Transportation Electrification. 2024, 10:3061-74. 10.1109/tte.2023.3304060
23. Qiao K, Sun P, Rong E, Sun J, Zhou H, Wu X: Anti-misalignment and lightweight magnetic coupler with H-shaped receiver structure for AUV wireless power transfer. IET Power Electronics. 2022, 15:1843-57. 10.1049/pel2.12352
24. Wang Z, Chen X, Jin X: A wireless power transmission system with high misalignment tolerance and high efficiency for autonomous underwater vehicles. Journal of Physics Conference Series. 2022, 2245:012007. 10.1088/1742-6596/2245/1/012007
25. Chen Z, Zhang X, Xu F, Li M, Yuan Z, Yang Q: Wide rotation-misalignment-tolerance design of magnetic coupled structure for AUVs wireless charging system. IEEE Transactions on Industrial Electronics. 2024, 71:14086-096. 10.1109/tie.2024.3382978
26. Li Z, Xie B, Zhu Y, Tang M, Liu H, Guo X, Sun H: Wireless charging constant power output system based on LCC/S-S self-switching. IEEE Access. 2022, 10:86435-444. 10.1109/access.2022.3199349
27. Wang X, Xu J, Leng M, Ma H, He S: A hybrid control strategy of LCC-S compensated WPT system for wide output voltage and ZVS range with minimized reactive current. IEEE Transactions on Industrial Electronics. 2021, 68:7908-920. 10.1109/tie.2020.3013788
28. Kandemir E, Borekci S: LCC-S compensated variable inductor-based hybrid topology analysis for inductive power transfer system. Electrical Engineering. 2023, 106:1585-604. 10.1007/s00202-023-02014-y
29. Makeen P, Ghali HA, Memon S: Theoretical and experimental analysis of a new intelligent charging controller for off-board electric vehicles using PV standalone system represented by a small-scale lithium-ion battery. Sustainability. 2022, 14:7396. 10.3390/su14127396
30. Makeen P, Ghali HA, Memon S, Duan F: Impacts of electric vehicle fast charging under dynamic temperature and humidity: experimental and theoretically validated model analyses. Energy. 2022, 261:125335. 10.1016/j.energy.2022.125335